ANALYSIS OF A GAS TURBINE ENHANCED FUEL CELL POWERTRAIN FOR FUTURE AIRCRAFT

Niclas A. Dotzauer*, Franciscus L.J. van der Linden*
* German Aerospace Center, Institute of System Architectures in Aeronautics, Münchener Straße 20, 82234 Weßling, Germany

Abstract

In this work, we present a novel idea of an SOFC combined with a gas turbine as the main powertrain of an aircraft. Contrary to similar, existing ideas, a pre-burner instead of a post-burner is used to heat up the gases before the fuel cell together with a hot air feedback. This allows for an autonomous start-up, the complete avoidance of air/air heat exchangers, which reduces weight and flow losses, and the use of high pressures, which is favorable for the operation of the SOFC. The investigations of this work are based on a dynamic Modelica model using components of the ThermoFluidStream (TFS) library, developed by the German Aerospace Center (DLR) with a custom fuel cell model following the TFS approach. To analyze the propulsion system, a preliminary control scheme is developed to perform simulations of an exemplary, regional aircraft over a whole mission while considering the different flight phases. First, a baseline case is simulated to investigate whether the system can be operated, also from the control perspective, and whether the performance is sufficient for the application in an aircraft. The results reveal that the system with the preliminary control loop achieves overall system efficiencies of up to 77% during the cruise phase. Second, simulations with different take-off temperatures and altitudes are carried out showing that the system runs robustly under more extreme conditions. These results show that the proposed architecture is very promising for aircraft applications.

Keywords

Aircraft Propulsion, Solid Oxide Fuel Cell, Gas Turbine, Dynamic Simulation, Control scheme

1. INTRODUCTION

Hydrogen technologies such as fuel cells can play a significant role in the decarbonization of future aircraft. Besides polymer electrolyte membrane (PEM) fuel cells, solid oxide fuel cells (SOFC) can be of high interest because the waste heat is produced at a much higher temperature level. This leads to better heat transfer properties allowing to use less or lighter heat exchangers, a possibility to partly transfer the residual heat into propulsive energy and to covering thermal loads, e.g. anti-icing.

Most early studies about SOFC in aviation investigated the substitution of conventional auxiliary power units (APU). The study of Mak and Meier [1] is a good example, stating that SOFCs have a weight disadvantage, which can be compromised by fuel savings and emission reduction due to possibly higher efficiencies. The analysis was performed based on simulations of replacing an APU sized for a 90 passenger more electric regional jet. Santarelli et al. [2] come to a similar conclusion for an SOFC system as APU in small, regional aircraft. Advantages over PEM fuel cells are the useful heat recovery and the flexibility to use hydrocarbon fuels as well as jet fuel. Although SOFCs have much higher startup times and thus would need to be put in standby during the aircraft being on the ground. Whyatt & Chick [3] provide an analysis especially on the weight of an SOFC power unit for the electrical loads of a Boeing 787 to investigate towards more electric aircraft. The most promising system with the SOFC being operated at a pressure of 8 bar and at a voltage of 0.825V was analyzed in more detail. The system was lighter than initially expected, but still over the referred 'breakeven weight' at which fuel would be saved compared to the conventional system. A broad overview of more studies on SOFC APU systems is given by the review of Fernandes et al. [4].

For stationary applications, the combination of gas turbines and SOFCs has been studied to a greater extent than for mobile applications. In Veyo et al. [5] different cycle configurations with the combination of tubular SOFCs and a gas turbine with an electric generator were investigated computationally and a test rig was built for proof of concept tests. The results indicate, that, the more complex the cycles are, the more efficient but also the more cost intensive they get. For example a simple cycle where the SOFC is operated at atmospheric pressure has less components but is also less efficient than a cycle with one low-pressure and one high pressure fuel cell stack using a two-staged compressor with intercooling. The integration of a pressurized stack with a micro gas turbine into a 200 kW test rig showed that the operation of such a

doi: 10.25967/650282

system is feasible with automatic start-up and operation control. This system had an overall efficiency of roughly 53% but, under some improvements, it is assumed to get to an efficiency of about 60%. Panne et al. [6] numerically analyzed similar cycles. Additionally to the results of [5], they came to the conclusion that the less complex systems also have a wider operating range, especially concerning the pressure ratio. Furthermore, the fuel flexibility was studied, which has little influence on the electric power output of the systems and some effect on the thermal power. Another interesting concept was investigated by Milcarek & Ahn [7] by the integration of micro-tubular SOFCs into a combustor with a fuel-rich and a fuel-lean combustion zone operated in series. The main advantage is the potential for a fast startup of the system within several minutes. Hence, it is possible to integrate this technology into jet engines.

In this work, a novel idea of an SOFC combined with a gas turbine as the main power source is presented, together with a prototypic control architecture. Contrary to similar ideas from literature, a pre-burner instead of a post-burner is used together with a recirculation path from the fuel cell exhaust air to the fresh air. This allows the pre-heating of the SOFC to operation temperature without external equipment. Further expected advantages are a complete avoidance of air/air heat exchangers, which reduces weight and flow losses, an easy startup of the system using the pre-burner and the use of high pressures, which is favorable for the operation of the SOFC.

In Figure 1, a possible integration in the nacelle of an aircraft is displayed. The system described above including a two-stage compressor, the pre-burner, the SOFC, the hot air feedback, a two-stage turbine and air-hydrogen heat exchangers is complemented by a gearbox connecting an electric motor and a propeller to the propulsion system. Depending on the operating point, the motor can also be used as a generator to distribute electric power to other systems in addition to the power supplied by the fuel cell. The idea behind the proposed hybrid powertrain architecture is to attach one larger nacelles to each wing of the aircraft. These two nacelles provide enough power for several smaller nacelles with only one engine to form a distributed propulsion system. During the normal operation of this hybrid system, most of the thermal power is provided by the fuel cell and only a fraction by the burner, which burns the excess hydrogen of the fuel cell exhaust gas.

The goal of this work is answering two questions. First, can the system be integrated and operated, also from a control point-of-view? Second, can this powertrain be useful for aviation concerning its operability in different conditions as well as its performance? This is done by conducting dynamic system-level simulations with regards to a possible control scheme over the whole mission range of an exemplary aircraft in different ambient temperatures and take-off altitudes.

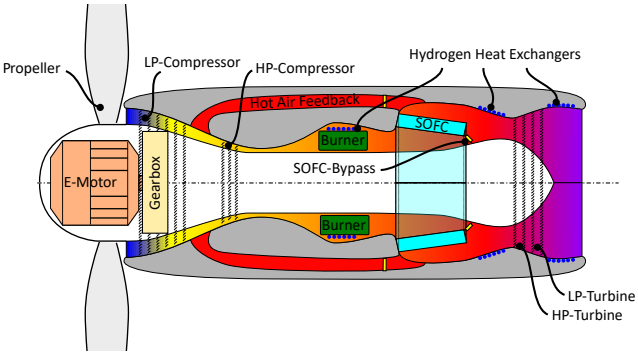

FIG 1. Symbolic nacelle integration of the powertrain including the air flow, the hydrogen flow is not shown in this layer.

2. SIMULATION SETUP

The system presented above is challenging to control because of the sensitivity of the SOFC, the large number of actuators, the high influence of the SOFC itself on the system and the strict temperature gradients, which have to be complied. Hence, a prototypical control system is developed for the explained powertrain architecture. This control will be based on a dynamic simulation model in Modelica. Herefore, the in-house developed, open-source library ThermoFluidStream (TFS) of the German Aerospace Center (DLR) provides an appropriate framework. The included, principle-based models enable robust simulations to estimate the dynamic behaviour of the whole fuel cell system and to analyze the performance over a whole flight mission.

2.1. Modeling Approach

Components from the TFS library and a custom fuel cell model following the TFS approach are used to model the proposed architecture. The Modelica model is presented in Figure 2, where parts such as sensors and flow resistances were left out for visualization purposes. In the hydrogen subsystem, marked by the green envelope, a source provides gaseous hydrogen at 23.15 K, which is just above the boiling temperature of 21.15 K [8]. After introducing heat from the burner via a conduction element, the fuel is compressed to a pressure of 10 bar. In streamwise direction, the flow is separated into two paths, one leading to an air-hydrogen heat exchanger to further heat up the hydrogen and the other bypassing this heat exchanger. The recombined flow then enters the fuel cell. The fuel cell anode exhaust gas including unused fuel and steam is burned. Note that a recirculation would need humidity management, which is deemed to be too heavy for aircraft applications. In the air subsystem, marked by the blue envelope, a source provides air, which is compressed to 10 bar as well before it flows through the burner. After the fuel cell, heat is transferred from the exhaust air to the hydrogen path in the heat exchanger. Further downstream the flow is separated into two parts. One path is the hot air feedback, which is mixed with

the air after the compressor and before the burner to heat up the fresh air stream. This is possible because of a highly over-stoichiometric air flow, which is used for the thermal management of the fuel cell. The other path leads to the turbine and ultimately to the outlet. The media models of hydrogen, air and water are taken from the TIL Media Suite [9] while being adapted to the use within the TFS library. Pure hydrogen is used from the source to the fuel cell. In every other component, a gas mixture of water vapor, hydrogen, oxygen and nitrogen is employed. Instead of the electrical part of a possible powertrain, a variable resistor is connected to the fuel cell to represent a load.

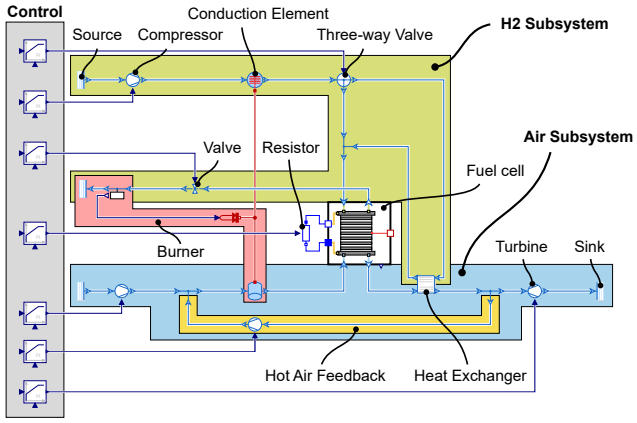

FIG 2. Simulation model of the fuel cell system including the control (grey), the hydrogen subsystem (green) and the air subsystem (blue). This is a simplified version of the simulation model used for visualization purposes.

Obvious simplifications are the lack of a hydrogen tank and the part of the hydrogen conditioning, where it is transformed from the liquid to the gaseous state. Additionally, components for a safe operation of the fuel cell such as emergency valves are not considered yet. The simplified burner, highlighted in red, is currently modeled by introducing heat into the air flow. The heat flux $\dot{Q}_{burner}$ is calculated by

$$\dot{Q}_{burner} = \dot{m}_{H2,burner} \cdot HHV_{H2} \tag{1}$$

with the mass flow of consumed hydrogen $\dot{m}_{H2,burner}$ and the higher heating value of hydrogen $HHV_{H_2} = 141.7$ MJ/kg.
The fuel cell model considers different physical aspects. The thermodynamics are covered by introducing one fluid volume for each electrode following the TFS approach. The masses of the different components of the gas mixture model change according to in- and outgoing mass flows. Fick's diffusion law is used to calculate the mass flow to the membrane. Distinct from the latter, the mass flow of consumed hydrogen $\dot{m}_{H_2,cons}$ is linked to the electric current i by Faraday's law of electrolysis:

$$i = \frac{z_{H2} \cdot F}{M_{H2} \cdot N_{cells}} \cdot \dot{m}_{H2,cons}, \tag{2}$$

where z_{H2} is the number of electrons per molecule of hydrogen, F the Faraday constant, M_{H2} the molar mass of a hydrogen molecule and N_{cells} the number of cells. The open circuit voltage U_{OCV} is computed by the Nernst equation including the standard-state reversible voltage E^0, a temperature-dependent term and a pressure-dependent term.

$$U_{OCV} = E^0 - e_T \cdot (T - T_0) - \frac{RT}{2F} \cdot ln\left(\frac{p_{H2O}}{p_{H2} \cdot \sqrt{p_{O2}}}\right) \tag{3}$$

The parameter e_T is an empirical parameter, $T - T_0$ the difference between fuel cell and reference temperature, R the universal gas constant and the normalized pressures p_X of water vapour, hydrogen and oxygen, respectively. To evaluate the cell voltage, the difference of open circuit voltage and three different voltage losses is calculated as

$$U_{cell} = U_{OCV} - \eta_{act} - \eta_{ohm} - \eta_{con}. \tag{4}$$

The activation losses

$$\eta_{act} = \frac{RT}{\alpha_c 2F} \cdot ln\left(\frac{j}{j_0}\right) \tag{5}$$

are dominant for low current densities j whereas α_c is the symmetry factor of the reaction and j_0 is the exchange current density. The ohmic losses, dominant for moderate current densities, are assessed by

$$\eta_{ohm} = ASR \cdot j \tag{6}$$

with the temperature-dependent area specific resistance defined as

$$ASR = \frac{T}{B_{ohm}} exp\left(\frac{E_{act,ohm}}{RT}\right) \tag{7}$$

from [10]. Hereby, B_{ohm} is a material-specific constant and $E_{act,ohm}$ the activation energy. The concentration losses

$$\eta_{act} = c_{con} \cdot ln\left(\frac{j_{lim}}{j_{lim} - j}\right), \tag{8}$$

dominant at high current densities, are currently implemented with a generalized approach from [11] using the parameter c_{con} and the limit current density j_{lim}, which are both empirical parameters. For the empirical and the material-dependent parameters, some assumptions are made to obtain an estimated performance of SOFC technology available for an entry into service of the aircraft in 2050.

2.2. Control Scheme

For this system, a control logic based on seven controllers is implemented. In the hydrogen system, the fuel cell inlet pressure and the mass flow have to be controlled to ensure the operation of the fuel cell and the burner. For now, this is realized by the combination of a compressor after the conduction element and a valve at the burner inlet. Additionally, the by-

pass over the heat exchanger is used to adjust the temperature of the hydrogen at the fuel cell inlet to the same level as the air temperature at the fuel cell inlet. Similarly to the hydrogen system, the fuel cell inlet pressure and the mass flow of the air system are controlled, not only for the operation of the fuel cell, but also for its thermal management. The latter is realized by balancing the combination of a highly over-stoichiometric inlet air flow, which has a cooling effect, and the recirculation air flow, which has a heating effect. For now, it is assumed that a lower concentration of around 15% mass to 18% mass of oxygen in the air, caused by the recirculation and the burner, doesn't have a large effect on the fuel cell performance. Furthermore, the electric resistor is controlled to influence the operating point of the fuel cell to obtain a desired power output. The control of the presented system is complex, as the different control-loops influence each other. For example, if less power is requested by the electrical system, the mass flows of fuel and air being needed for the operation are lower, because the operating point of the fuel cell stack changes. Simultaneously, the efficiency increases, which results in less heat being produced. Hence, the thermal management is affected as well.
The controllers in the current stage of the system are implemented as PI controllers. An overview of the set points is given in Table 1. The inlet pressure into the fuel cell stack is denoted as $p_{k,in}$ for each species Hydrogen (H2) and Air. Accordingly, λ_k refers to the surplus ratio, $T_{k,in}$ to the inlet temperature and $P_{el,FC}$ to the electric power output of the fuel cell stack. The surplus ratio is defined as

$$\lambda_k = \frac{\dot{m}_{k,in}}{\dot{m}_{k,cons}} \tag{9}$$

with the inlet mass flow $\dot{m}_{k,in}$ and the consumed mass flow $\dot{m}_{k,cons}$ of the species k. Thus, the control of the surplus ratio is effectively a control of the mass flow. This is important for the integration, as the surplus ratio can not be measured in a real system as opposed to the mass flow. For this first analysis of the system, the air compressor and the turbine are not coupled, which would not be the case in a real system. This is done for an easier control of the system without the need of properly sizing the compressor and the turbine together.

3. RESULTS AND DISCUSSION

In the first part of this section, a baseline mission simulation is carried out with the presented simulation setup. Starting at sea level with an ambient temperature of 15 °C, the international standard atmosphere (ISA) is assumed to calculate the altitude-dependent air properties. The altitude profile is depicted in Figure 6a over the whole duration of the mission. Different phases are considered with a peak altitude of 7620 m or 25000 ft, which is the ceiling service altitude for many common turboprop aircraft, and a go-around altitude of 2560 m (8000 ft) added to the landing altitude. The performance of the proposed powertrain architecture over the baseline mission is analyzed.
In the second part of this section, simulations with extreme conditions such as high and low ambient temperatures and a high take-off altitude are performed. The results are then compared to the baseline case. Hereby, possible improvements of the powertrain for future iterations are discussed.

TAB 1. Overview of the control scheme with the control variables, their set points and the corresponding actuators.

Variable	Set point	Actuator
$p_{H2,in}$	10 bar	Hydrogen compressor
$p_{Air,in}$	10 bar	Fresh air compressor
λ_{H2}	1.15	Burner inlet valve
λ_{Air}	4	Turbine
$T_{H2,in}$	650 °C	Hot air feedback compressor
$T_{Air,in}$	650 °C	Three-way valve
$P_{el,FC}$	various	Resistor

3.1. Baseline Mission

For the operation of the fuel cell, among other aspects, suitable temperatures of the reactants have to be provided. A detailed view of the temperatures at various locations during the cruise phase is displayed in Figure 3. As mentioned above, the ground temperature for the baseline mission is set to 15 °C resulting in a temperature of -34.5 °C at cruise altitude, which is the inlet temperature at the source. Compressing the air to 10 bar has a large effect on the temperature. Together with the hot air feedback and the heat of the burner, the inlet temperature of the fuel cell is set to 650 °C. The increased temperature after the fuel cell is lowered again in the air-hydrogen heat exchanger and in the turbine before reaching the exhaust. The hydrogen enters the associated subsystem in a gaseous state at a temperature of 23.15 K or -250 °C. After heating up the fuel by the conduction element and the compression, the fuel cell inlet temperature of the hydrogen is set to the same value as the air. This is achieved by adjusting the flow rate over the bypass with the air-hydrogen heat exchanger. The operating temperature of the SOFC is 810 °C, which is not shown in the figure, lying well within the desired range of 600 °C to 1000 °C. The stack temperature during the flight varies from 793 °C in the end of the descent phase to 817 °C after take-off. This is already good for this simple control approach. However, there is potential for optimization regarding the strict temperature gradients for SOFCs of around 5-10 K/min [12]. Especially in the transition from taxi to flight and vice versa, the temperature gradients reach levels of over 100 K/min. In the current system only the fuel cell inlet temperature is controlled. Therefore,

the control loop should be optimized for a better thermal management.

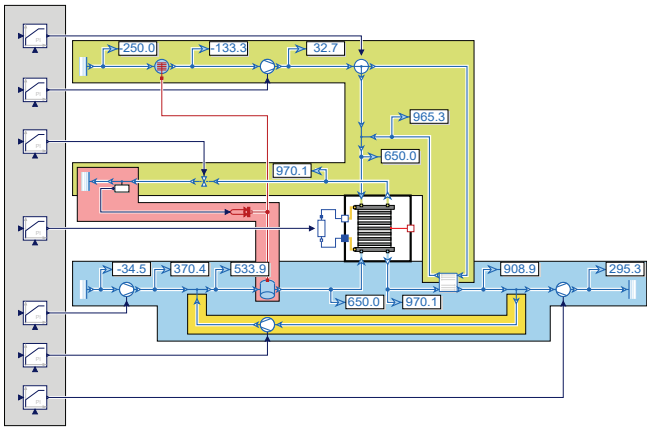

FIG 3. Temperatures in °C at various locations of the architecture, shown in a simplified version of the simulation model for visualization purposes.

Over the mission duration, different electrical power levels are requested from the fuel cell ranging from 200 kW during the taxi phase to the peak demand of 1 MW during take-off. This is displayed as $P_{el,stack}$ in Figure 4 together with the total chemical input power

$$P_{ch,tot} = \dot{m}_{cons,tot} \cdot LHV_{H_2}, \tag{10}$$

where $\dot{m}_{cons,tot}$ is the mass flow of consumed hydrogen by burner and fuel cell combined and LHV_{H_2} is the lower heating value of hydrogen. It is assumed, that water is completely vaporized, because the temperatures are well above the dew point of 180 °C at 10 bar pressure [13]. Hence, the use of the lower heating value is justified. Also shown in Figure 4 is the effective mechanical power, which is computed by the difference of the power output of the turbine and the power input of the three compressors:

$$P_{mech,eff} = P_{turbine} - \sum_{i=1}^{3} P_{compressor,i}, \tag{11}$$

assuming a combined operation without any losses. Together with the net power output

$$P_{net} = P_{el,stack} + P_{mech,eff}, \tag{12}$$

the impact of the pressurization and the mechanical components using the heat of the burner and the fuel cell is illustrated. Over the mission, the ratio of the effective mechanical power and the net power output

$$r_{P,mech} = \frac{P_{mech,eff}}{P_{net}}. \tag{13}$$

slightly varies around 20% as seen in Figure 5. The ratio ranges from 21% during the climb to 14% during the landing. Only in the taxi phases $r_{P,mech}$ is very low. For these phases, a better operational point might be found in the future. For the majority of the mission duration, however, it makes sense to pressurize the system. This is affirmed by the overall system

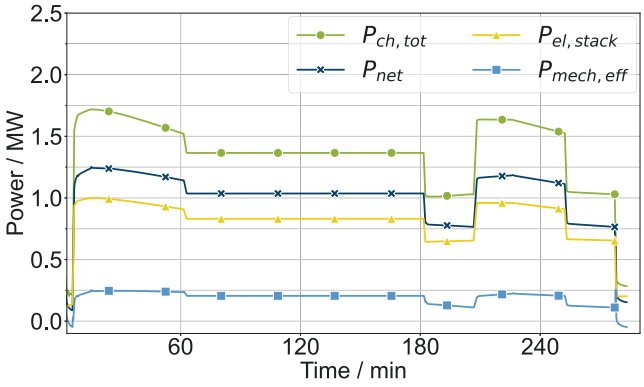

FIG 4. Total chemical power of the system, electrical power output of the SOFC, effective mechanical power output of the compressors and the turbine and net power output of the complete system.

efficiency depicted in Figure 5:

$$\eta_{sys} = \frac{P_{net}}{P_{ch,tot}}. \tag{14}$$

Additionally to poviding power, the integration of the pressurization also increases the system efficiency compared to the SOFC stack efficiency. The latter is evaluated by

$$\eta_{stack} = \frac{P_{el,stack}}{P_{ch,stack}}, \tag{15}$$

where

$$P_{ch,stack} = \dot{m}_{cons,stack} \cdot LHV_{H_2} \tag{16}$$

with the hydrogen mass flow consumed by the stack $\dot{m}_{cons,stack}$. When evaluating the cruise phase, for example, the system efficiency at 76% is 6% higher than the stack efficiency at 70% during this phase. Pressurization also allows for a smaller, lighter fuel cell stack, which is essential for the application in an aircraft. Although it is not the focus of this work, there will be a trade-off between SOFC weight and pressure level as the balance of plant components such as the compressors and the turbine get heavier and larger with an increasing pressure level. This was shown by [14] for PEM fuel cells in aviation. Although the PEM fuel cell system differs from an SOFC system, the dependencies of the pressurization are similar.

3.2. Varying Ambient Conditions

The operation of the powertrain of an aircraft has to be ensured not only for standard conditions such as in the baseline mission, but also for more extreme conditions. To analyze the behaviour and the performance of the proposed powertrain architecture, three different cases are considered with the specifications shown in Table 2. The names refer to the city or airport with the correspondent conditions. These airports are also included in extreme weather tests of

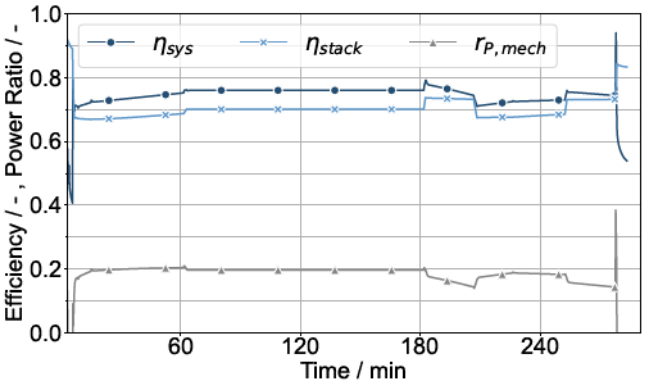

FIG 5. Fuel cell stack efficiency, overall system efficiency and share of the mechanical power in the net power output.

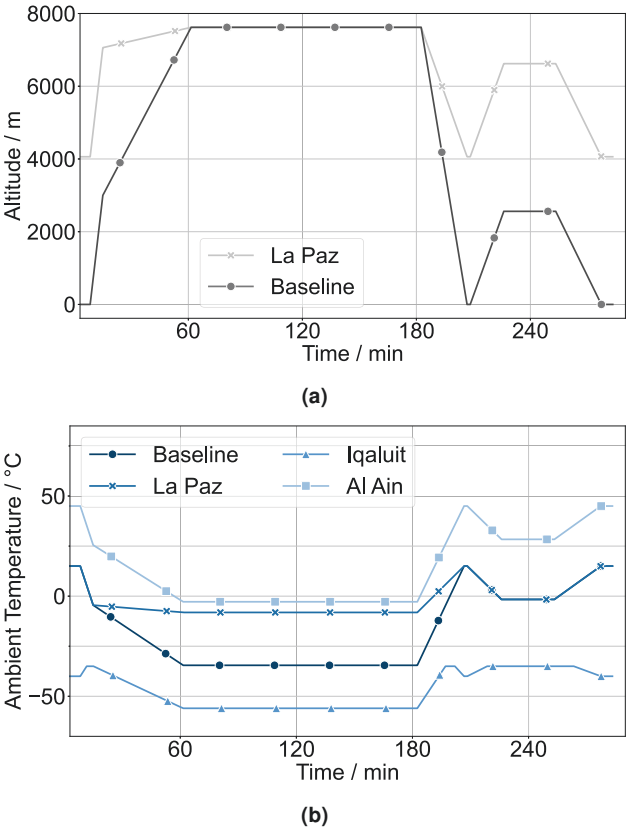

FIG 6. Mission profiles: a) Altitude profile for the baseline and the La Paz case. The Iqaluit and the Al Ain cases are not shown, because they are almost the same as the baseline case. b) Temperature profiles for all missions.

new commercial aircrafts such as the Airbus A350 [15].

The landing and take-off altitudes are set to the same value in each mission for a more meaningful analysis. The full altitude profiles are presented in Figure 6a. Since the altitude of the Iqaluit and Al Ain cases, presented in Table 2, are almost the same as the baseline case, they are not included in the figure for better visibility. The corresponding temperatures are displayed in Figure 6b. Note that the ambient temperatures over Arctica don't follow the ISA function. Therefore, the temperatures for the Iqaluit case are taken from [16] with a ground temperature of -40°C following the temperatures of the arctic minimum. For the other cases, the basic ISA function should be a good approximation of real-world conditions. [17].

When analyzing the power output, there are only small transient deviations between the electrical power of the fuel cell for the different missions since this is a controlled variable. Similarly, the stack efficiency remains almost the same when varying the ambient conditions by controlling the inlet pressure, the inlet temperature and the surplus ratio to a constant value. In addition, the consumed mass flow by stack and burner combined is at the same level and therefore also the total chemical input power (see Equation 10). The only major differences appear for the effective mechanical power output depicted in Figure 7a and for the overall system efficiencies in Figure 7b. Analyzing the effective power, the highest power output appears for the Iqaluit case with the lowest temperatures, followed by the baseline case. This can be explained by the Joule-Brayton process, which, in general, yields a higher power output for lower ambient temperatures. In flight phases with low altitudes, i.e. in the beginning of the climb, towards the landing and during the go-around, the effective mechanical power of the La Paz case is slightly higher than the one of the baseline case. Here, another working principle of the Joule-Brayton process applies, where the power output is also higher for higher pressure ratios. At the same ambient temperature, the pressure ratio in the La Paz case is higher than in the baseline case due to lower ambient pressures. Regarding these relations, the Al Ain case has the lowest power output due to higher ambient temperatures and similar ambient pressures as e.g., the baseline case. This agrees with the simulation results. At high altitudes, however, the power output of the La Paz case is almost as low as the one of the Al Ain case. This can be explained by the ambient pressure being the same and the temperature levels being similar.

The overall system efficiencies observed in Figure 7b follow the results of the mechanical power output. While the latter contributes to a higher net power output, the total chemical power input remains almost the same between the different missions, as explained above. One difference hereby is, that the efficiency is lower for high power outputs. However, the overall efficiencies are quite high, reaching values from 74.4% up to 77% during the cruise phase and still being above 70% during take-off.

4. CONCLUSION

This work analyzed a possible integration of a gas turbine enhanced SOFC powertrain for the application in future aircraft. A dynamic, system-level simulation model was developed using the TFS library

TAB 2. Specifications of the performed mission simulations.

Name	Location	Ground altitude	Ground temperature	Sea level temperature
Baseline	Generic	0 m	15°C	15°C
La Paz	El Alto, Bolivia	4061 m	15°C	41.4°C
Iqaluit	Iqaluit, Canada	34 m	-40°C	-40.2°C
Al Ain	Al Ain, UAE	264 m	45°C	46.7°C

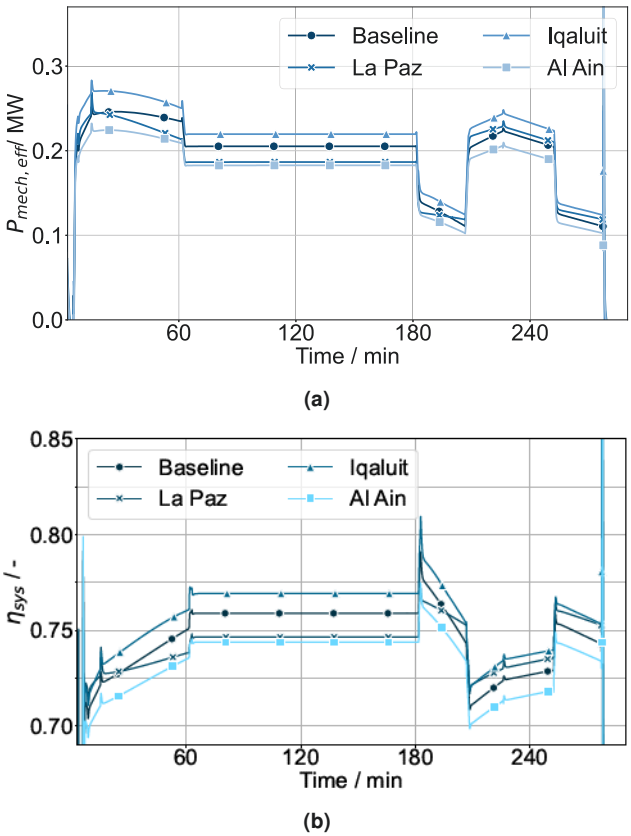

FIG 7. Major differences when varying the ambient conditions: a) Effective mechanical power output of the compressors and the turbine for the different missions. b) Overall system efficiencies for the different missions.

and a custom fuel cell model in Modelica. This was done to investigate the behaviour of the fuel cell and the balance of plant components needed for its operation. A first control scheme was introduced with which it was possible to perform simulations over the complete mission duration of an aircraft. Key aspects of the dynamics were included while keeping CPU times low. The first goal of this work was to show the feasibility of operating the proposed powertrain architecure, also from the control perspective, which was achieved by performing the mission simulations. The second goal was to investigate, whether the system can be useful for the application in aviation, regarding both, the operability in different conditions and also the performance. The results show, that the powertrain performs well under various extreme conditions, which are used for testing commercial aircraft. Simultaneously, high overall system efficiencies of up to 77% were achieved, exceeding the efficiencies of state-of-the-art conventional jet engines. Although the model represents a more principle-based approach, the results are a promising outcome for this architecure. Towards a real integration, however, many aspects have to be considered, e.g. concerning a reliable and safe operation. Future iterations of the simulation setup might include optimizations such as the exact position of heat exchangers in the architecture or optimizing the operating points, also for different flight phases. It would also be interesting to look into the startup phase in more detail. Furthermore, the control scheme should be improved to handle more complex situations and for a better thermal management while being real-time compatible. Additional features of the simulation setup might include emergency bypasses around the SOFC stack to enable a safe operation, consider the hydrogen conditioning featuring a tank and a vaporizer and connecting the stack to an electrical system. Moreover, a more elaborate burner model is desired in order to analyze the oxygen concentration through the air cycle. Especially for an integration in future aircraft, the component masses and dimensions have to be considered as well.

References

[1] Audie Mak and John Meier. Fuel cell auxiliary power study volume 1: Raser task order 5. Technical report, 2007.

[2] Massimo Santarelli, M Cabrera, and M Calì. Analysis of solid oxide fuel cell systems for more-electric aircraft. *Journal of aircraft*, 46(1):269–283, 2009.

[3] Greg A Whyatt and Lawrence A Chick. Electrical generation for more-electric aircraft using solid oxide fuel cells. Technical report, Pacific Northwest National Lab.(PNNL), Richland, WA (United States), 2012.

[4] Marina Domingues Fernandes, ST de P Andrade, Victor Nikolaus Bistritzki, Rafaela Marinho Fonseca, LG Zacarias, HNC Gonçalves, Adler Fonseca de Castro, Rosana Zacarias Domingues, and Tulio Matencio. Sofc-apu systems for aircraft: A review. *International Journal of Hydrogen Energy*, 43(33):16311–16333, 2018.

[5] Stephen E Veyo, Wayne L Lundberg, Shailesh D Vora, and Kevin P Litzinger. Tubular sofc hybrid

power system status. In *Turbo Expo: Power for Land, Sea, and Air*, volume 36851, pages 649–655, 2003.

[6] Tobias Panne, Axel Widenhorn, Manfred Aigner, and Marcello Masgrau. Operation flexibility and efficiency enhancement for a personal 7kw gas turbine system. In *Turbo Expo: Power for Land, Sea, and Air*, volume 48852, pages 1–12, 2009.

[7] Ryan J Milcarek and Jeongmin Ahn. Rich-burn, flame-assisted fuel cell, quick-mix, lean-burn (rfql) combustor and power generation. *Journal of Power Sources*, 381:18–25, 2018.

[8] Yiming Zhang, Julian RG Evans, and Shoufeng Yang. Corrected values for boiling points and enthalpies of vaporization of elements in handbooks. *Journal of Chemical & Engineering Data*, 56(2):328–337, 2011.

[9] Tilmedia suite - software package for calculating the properties of thermophysical substances. https://www.tlk-thermo.com/fileadmin/user_upload/SoftwareFiles/TILMedia/TILMedia_Suite_EN_2020_September.pdf, 2020. TLK-Thermo GmbH, Accessed: 2024-06-20.

[10] J-C Njodzefon, D Klotz, A Kromp, A Weber, and E Ivers-Tiffée. Electrochemical modeling of the current-voltage characteristics of an sofc in fuel cell and electrolyzer operation modes. *Journal of The Electrochemical Society*, 160(4):F313, 2013.

[11] Ryan O'hayre, Suk-Won Cha, Whitney Colella, and Fritz B Prinz. *Fuel cell fundamentals*. John Wiley & Sons, 2016.

[12] Zezhi Zeng, Yuping Qian, Yangjun Zhang, Changkun Hao, Dan Dan, and Weilin Zhuge. A review of heat transfer and thermal management methods for temperature gradient reduction in solid oxide fuel cell (sofc) stacks. *Applied Energy*, 280:115899, 2020.

[13] Peter Stephan, Stephan Kabelac, Matthias Kind, Dieter Mewes, Karlheinz Schaber, and Thomas Wetzel. *VDI-Wärmeatlas: Fachlicher Träger VDI-Gesellschaft Verfahrenstechnik und Chemieingenieurwesen*. Springer-Verlag, 2019.

[14] Matthias Schröder, Florian Becker, Josef Kallo, and Christoph Gentner. Optimal operating conditions of pem fuel cells in commercial aircraft. *International Journal of Hydrogen Energy*, 46(66):33218–33240, 2021.

[15] Test and certification - approvals for entry-in-service. https://www.airbus.com/en/products-services/commercial-aircraft/the-life-cycle-of-an-aircraft/test-and-certification. Airbus, Accessed: 2024-06-18.

[16] Dominic J Diston. *Computational modelling and simulation of aircraft and the environment, volume 1: Platform kinematics and synthetic environment*, volume 1. John Wiley & Sons, 2009.

[17] Mustafa Cavcar. The international standard atmosphere (isa). *Anadolu University, Turkey*, 30(9):1–6, 2000.